

Waves in THF hydrate-bearing sands

Jongchan Kim¹, Yongkoo Seol², Sheng Dai^{1*}

¹*Geosystems Engineering, Georgia Institute of Technology, Atlanta, GA 30332 USA*

²*National Energy Technology Laboratory, US Department of Energy, Morgantown, WV 26507 USA*

*Corresponding author: sheng.dai@ce.gatech.edu

Abstract

The stiffness of hydrate-bearing sediments are governed by confining stress and hydrate saturation, and largely affected by hydrate pore habits and distribution. This study experimentally determines the P- and S-wave velocities in sands with various THF hydrate saturations. Results show that the Poisson's ratio of hydrate-bearing sands decreases from nearly $\nu=0.5$ in sediments with no hydrate to $\nu \sim 0.3-0.35$ at fully hydrate saturated condition. The simultaneous measurement of both P- and S-wave velocities allows the determination of all small-strain elastic (Young's, bulk, constrained, and shear) moduli in hydrate-bearing sediments. Results of all elastic properties of hydrate-bearing sediments with various saturations provide essential information for hydrate simulators.

1. Introduction

Accurate understanding of hydrate formation and dissociation processes on physical properties of hydrate-bearing sediments is essential to economic and safe exploitation of gas hydrate as a potential energy resource. Most hydrate saturation dependent physical properties of hydrate-bearing sediments are largely affected by not only the pore volume fraction but also the pore habits of the hydrate in sediments. The morphology of naturally occurred hydrate in sediments is mainly governed by the relative magnitude of capillarity and skeleton forces, rendering pore-filling or segregated as veins, nodules, or chunks [1, 2]. Hydrate pore habits synthesized in laboratory specimens depend on hydrate formation methods [3], resulting in physical properties varying several orders of magnitude even with identical hydrate saturation in sediments.

Wave characterization of hydrate-bearing sediments provides information on small-strain stiffness and estimation of hydrate saturation [4] and morphology [5, 6]. Oceanic seismic survey uses P-wave for hydrate deposit characterization [7] as water does not transmit shear energy. Laboratory characterization of hydrate-bearing sediments mainly use S-wave as it reflects the properties of the soil skeleton and P-wave is largely affected by the presence of air even with a small volume fraction [8]. Elastic wave velocities, i.e., essentially the small-strain stiffness of hydrate-bearing sediments, increase with hydrate saturation, yet the increasing trends vary by hydrate distribution and morphology at the pore- and core-scales [5, 6, 9, 10]. Current laboratory studies use either P- or S-wave to characterize hydrate-bearing sediments and fail to deploy P- and S-waves simultaneously [9, 11], although by doing so all small-strain elastic moduli including the Poisson's ratio can be determined. This study experimentally investigates the hydrate saturation dependent elastic moduli and Poisson's ratio of hydrate-bearing sands by simultaneous measurement of P- and S-wave velocities.

2. Experimental Design

2.1 Experimental setup

An aluminum cell (inner diameter = 0.8 inch or 20.32mm) is used for this study. The top and bottom pedestals are equipped with a pair of piezo disks and bender elements for p- and s-wave measurement. Wave signals from the bottom piezo crystals, generated and modulated from a function generator (Agilent 34970A), propagate through the specimen upwardly, and are detected by the top piezo crystals. Received signatures are filtered and amplified (Krohn-Hie 3361) before being displayed and saved on an oscilloscope (Agilent DSOX2004A). The temperature is continuously monitored using two T-type thermocouples embedded within the sediments. The whole setup is placed within a walk-in refrigerator (Darwin Chambers) with a resolution of 0.1°C for temperature control during hydrate

formation and dissociation.

2.2 Specimen preparation

F110 quartzitic fine sands (mean grain size $d_{50}=120\mu\text{m}$, maximum and minimum porosity $e_{max}=0.848$ and $e_{min}=0.545$) are used to make the specimen. Tetrahydrofuran (THF) is adapted as a hydrate former substance in this study, due to its high solubility in water, ease control of hydrate saturation, and relatively short period of hydrate formation [12]. Hydrate saturations (i.e., $S_h = 0.3, 0.6,$ and 1 in this study) are controlled by making stoichiometric solutions with corresponding mass ratios of THF and deionized water. After well mixing of the stoichiometric solution with F110 sands, they are scooped into the aluminum cell. All specimens are fully saturated and packed to a relative density of $D_r = 40\%$ with a height of 1 inch (25.4mm). A vertical stress of 90kPa is applied on the top pedestal and remain constant throughout the tests.

The whole setup is then placed into the refrigerator and the temperature is lowered to 1°C to trigger hydrate formation, which can be indicated by the measured thermal peak as shown in Figure 1. The P- and S-waves are continuously measured throughout this process.

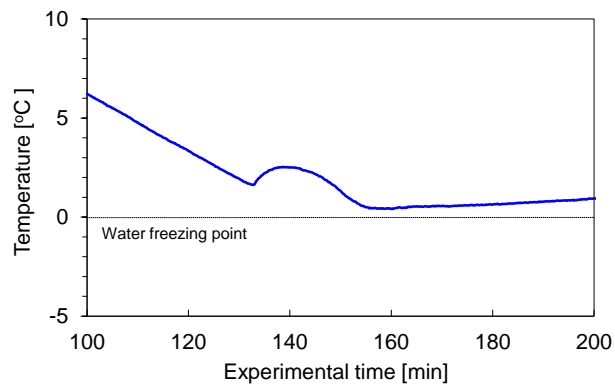


Figure 1: Temperature change during the formation of THF hydrate in sediments ($S_h=1$ in this case).

3. Results and Analysis

Figure 2 shows the collected P- and S-wave signatures during hydrate formation and dissociation in all tested specimens. All wave are measured in specimens under a vertical stress of 90kPa. Hydrate formation rapidly shortens the direct wave travel time from the source to the receiver and thus with a higher velocity; inversely, hydrate dissociation slows both P- and S-wave velocities, suggesting significant stiffness reduction in sediments is expected during gas production.

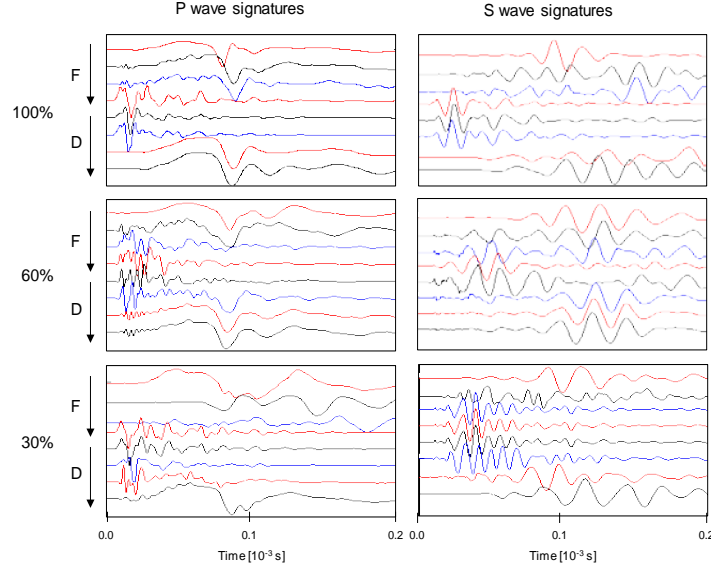


Figure 2: P- and S- wave signatures during hydrate formation and dissociation in sediment with different hydrate saturations. F and D represent hydrate formation and dissociation respectively.

With known tip-to-tip distance of the piezo crystals and the direct wave travel times (Figure 2), the corresponding wave velocities can be determined (Figure 3). Both saturation dependent P- and S-wave velocities show an ‘S-shaped’ trend as in sediments with pore-filling or patchy hydrates in previous studies [2, 9, 13]. For hydrate formed in an saturated system, where water initially prefers residing at grain contacts, tends to form a cementing type hydrate-bearing sediments and thus the stiffness increases rapidly even with a small amount of hydrate [14-16].

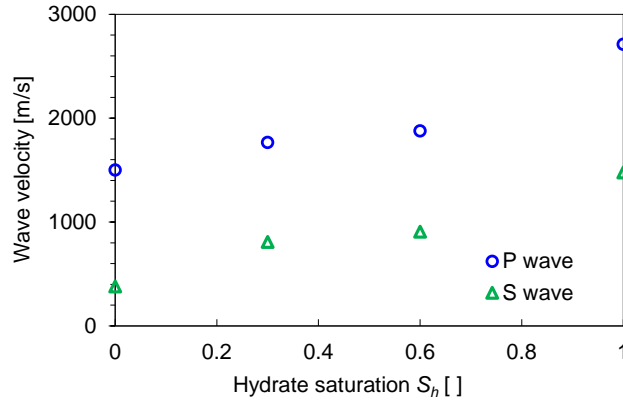


Figure 3: Measured P- and S-wave velocities in sediments with different THF hydrate saturations.

4. Analysis and Discussion

The specimen’s bulk Poisson ratio ν can be determined by knowing both P- and S-wave velocities:

$$\nu = \frac{\left(\frac{V_p}{V_s}\right)^2 - 2}{2\left(\frac{V_p}{V_s}\right)^2 - 2} \quad (1)$$

Figure 4 plots the hydrate saturation dependent Poisson’s ratio, compared with previous experimental data and those obtained from various geophysics models. The contact-cementing, grain-coating, loading-bearing, and pore-filling models are based on [17, 18]; and the patchy model is based on the self-consistent model [19]. Apparently, elastic moduli and the Poisson’s ratio of hydrate-bearing sediments largely depend on hydrate pore habits. All

experimentally determined Poisson's ratio in THF hydrate-bearing sediments decreases with increasing hydrate saturation, generally follow the trends predicted by the loading-bearing and patchy models. Measured Poisson's ratios start from nearly $\nu=0.5$ with no hydrate to $\nu= \sim 0.3-0.35$ at fully hydrate saturated condition. This also implies increased soil skeletal stiffness with increased hydrate saturation. Note that the Poisson's ratio in [9, 11] are measured under nominal stress, while this study is conducted under 90kPa vertical stress.

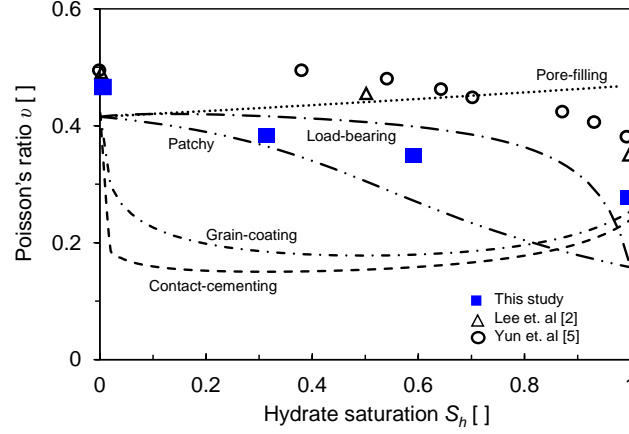


Figure 4: Poisson's ratio as a function of hydrate saturation.

Additionally, both P- and S-wave velocities inherently reflect the material moduli (i.e., stiffness) and density ρ , as shown below

$$V_p = \sqrt{\frac{M}{\rho}} = \sqrt{\frac{B + \frac{4}{3}G}{\rho}}, \quad (2)$$

$$V_s = \sqrt{\frac{G}{\rho}}, \quad (3)$$

where M , B , and G are constrained, bulk, and shear moduli. With known specimen density, all elastic moduli in sediments at various hydrate saturations are summarized in Table 1. Note that elastic moduli of granular materials increase exponentially with stress and all the reported values here are under 90kPa vertical stress at a zero-lateral strain condition.

Table 1: Poisson's ratio and elastic moduli of THF hydrate-bearing sands under 90kPa vertical stress.

Hydrate saturation, S_h [-]	0	0.3	0.6	1
Bulk Poisson's ratio, ν [-]	0.47	0.37	0.35	0.29
Shear modulus, G [GPa]	0.3	1.7	2.8	9.4
Constrained modulus, M [GPa]	4.4	8.1	11.9	31.8
Bulk modulus, B [GPa]	4.0	5.8	8.2	19.2
Young's modulus, E [GPa]	0.8	4.6	7.5	24.3

Conclusion

The stiffness of hydrate-bearing sediments are governed by confining stress and hydrate saturation, and largely affected by hydrate pore habits and distribution. P- and S-waves capture the bulk and shear stiffness of hydrate-bearing sediments, and the combination of the two allows the determination of all elastic moduli of hydrate-bearing sediments. Measuring P- and S-wave velocities in THF hydrate-bearing sands in this study concludes that the Poisson's ratio of hydrate-bearing sands decreases from nearly $\nu=0.5$ in water saturated sediments with no hydrate to $\nu= \sim 0.3-0.35$ at fully hydrate saturated condition; all elastic moduli increases with hydrate saturation; and these elastic properties of hydrate THF hydrate-bearing sediments can be better estimated using the loading-bearing or self-consistent models. Admittedly, effects of confining stress and gas content on these elastic properties need

further investigation.

References

- [1] Clennell BM, Hovland M, Booth JS, Henry P, Winters WJ. Formation of natural gas hydrates in marine sediments 1. Conceptual model of gas hydrate growth conditioned by host sediment properties. *J Geophys Res* 1999;104:22985-3003.
- [2] Dai S, Santamarina JC, Waite WF, Kneafsey TJ. Hydrate morphology: Physical properties of sands with patchy hydrate saturation. *Journal of Geophysical Research: Solid Earth* 2012;117:B11205.
- [3] Waite WF, Santamarina JC, Cortes DD, Dugan B, Espinoza DN, Germaine J, et al. Physical properties of hydrate-bearing sediments. *Rev Geophys* 2009;47:RG4003.
- [4] Lee MW. Models for gas hydrate-bearing sediments inferred from hydraulic permeability and elastic velocities. *US Geolog Survey Scientific Investigate Report* 2008;5219:15.
- [5] Priest JA, Rees EV, Clayton CR. Influence of gas hydrate morphology on the seismic velocities of sands. *Journal of Geophysical Research: Solid Earth* 2009;114.
- [6] Yun TS, Francisca FM, Santamarina JC, Ruppel C. Compressional and shear wave velocities in uncemented sediment containing gas hydrate. *Geophys Res Lett* 2005;32:L10609.
- [7] Dai J, Xu H, Snyder F, Dutta N. Detection and estimation of gas hydrates using rock physics and seismic inversion: Examples from the northern deepwater Gulf of Mexico. *The Leading Edge* 2004;23:60-6.
- [8] Santamarina JC, Klein A, Fam M. *Soils and waves*. New York: John Wiley & Sons; 2001.
- [9] Lee J, Francisca FM, Santamarina JC, Ruppel C. Parametric study of the physical properties of hydrate-bearing sand, silt, and clay sediments: 2. Small-strain mechanical properties. *Journal of Geophysical Research: Solid Earth (1978–2012)* 2010;115.
- [10] Winters WJ, Pecher IA, Waite WF, Mason DH. Physical properties and rock physics models of sediment containing natural and laboratory-formed methane gas hydrate. *American Mineralogist* 2004;89:1221-7.
- [11] Yun T, Francisca F, Santamarina J, Ruppel C. Compressional and shear wave velocities in uncemented sediment containing gas hydrate. *Geophysical Research Letters* 2005;32.
- [12] Lee J, Yun T, Santamarina J, Ruppel C. Observations related to tetrahydrofuran and methane hydrates for laboratory studies of hydrate-bearing sediments. *Geochemistry, Geophysics, Geosystems* 2007;8.
- [13] Spangenberg E, Kulenkampff J, Naumann R, Erzinger J. Pore space hydrate formation in a glass bead sample from methane dissolved in water. *Geophysical Research Letters* 2005;32.
- [14] Winters W, Waite W, Mason D, Gilbert L, Pecher I. Effect of grain size and pore pressure on acoustic and strength behavior of sediments containing methane gas hydrate. *Fifth International Conference on Gas Hydrates, Trondheim, Norway* 2005. p. 12-6.
- [15] Priest JA, Best AI, Clayton CRI. A laboratory investigation into the seismic velocities of methane gas hydrate-bearing sand. *J Geophys Res* 2005;110:B04102.
- [16] Chand S, Minshull TA, Priest JA, Best AI, Clayton CRI, Waite WF. An effective medium inversion algorithm for gas hydrate quantification and its application to laboratory and borehole measurements of gas hydrate-bearing sediments. *Geophysical Journal International* 2006;166:543-52.
- [17] Dvorkin J, Helgerud MB, Waite WF, Kirby SH, Nur A. Introduction to physical properties and elasticity models. *Natural Gas Hydrate* 2000:245-60.
- [18] Mavko G, Mukerji T. Bounds on low-frequency seismic velocities in partially saturated rocks. *Geophysics* 1998;63:918-24.
- [19] Berryman JG. Long-wavelength propagation in composite elastic media I. Spherical inclusions. *J Acoust Soc Am* 1980;68:6.